

Facile precipitation microfluidic synthesis of Monodisperse and inorganic hollow microspheres for Photocatalysis

Chunlin Li,^a Zhiyu Wang,^b Hua Xie,^a Jun Bao,^b Yingxu Wei,^a Bingcheng Lin^a and Zhongmin Liu^{a,c*}

Abstract

BACKGROUND: Hollow microspheres have potential applications for wide-range fields, especially photocatalysis, attracting tremendous attention in material science. However, conventional synthesis of hollow microspheres involves complicated procedures, high cost and poor yields, greatly impeding their development. Due to the limitations of raw material for the polymerization or hydrolysis routes so far the hollow materials prepared in a microfluidics chip were limited to some specific substances.

RESULTS: Herein, a controllable precipitating reaction strategy in droplets was presented to form the hollow structure from easily accessible industrial chemical materials (such as nitrates of Zinc, Copper and Cobalt, and Ferrous sulfate). After generating monodisperse droplets and followed introducing precipitant into the droplets in a microfluidics chip, the spherical shell was constructed through the accumulation of precipitated particles at the oil/water interface of droplets and further particle growth on the inner shell. As a result, hollow microspheres with a Janus shell of different inner and outer morphology were formed. The photocatalytic activities of these hollow microspheres were evaluated for RhB photodegradation oxidation based on heterogeneous photo-Fenton. The photocatalytic activities of the fresh hollow samples showed better than their solid samples or their oxidized hollow samples.

CONCLUSION: With microfluidic technology, the transition-metallic inorganic hollow microspheres can be rapid, low-costly manufactured through direct precipitation reaction in droplets. The prepared α -Co(OH)₂ hollow microspheres showed promising photocatalytic activity.

© 2021 Society of Chemical Industry (SCI).

Keywords: microfluidics; hollow microsphere; heterogeneous Fenton; controllable synthesis; photocatalysis

INTRODUCTION

Hollow microspheres, especially monodisperse, have attracted considerable interest in the past few decades,^{1–3} due to their distinctive properties, such as well-defined morphology, uniform size, low density, and valuable void space. They have potential applications in wide range of fields, such as catalysis,^{4–9} sensing,^{10,11} adsorbent,^{12,13} energy,^{14–17} biomedical applications,^{18,19} etc. Via multiple scattering by the inner surface of the hollow material, hollow structure may improve the overall light absorption efficiency,^{20–22} thereby attracting especially attention in photocatalysis.

A wide variety of chemical and physicochemical methods have been developed to synthesize the hollow structure of the micrometer or nanometer.^{1,2,6,14,23} The most common synthesis route was carried out in a liquid medium with a hard or soft template.^{24–28} A typical synthesis procedure was basically operated in a highly diluted media in a batch reactor, involving the processing of large volumes of feed and the poor yields of the target product. Thus the synthesis procedure was usually low efficiency and high cost. Moreover, the syntheses procedures in most protocols were often rather intricate and multistep operations,

resulting in miserable operational applicability, bad reproduction, and poor homogeneity. Therefore, a facile and continuous route to produce monodisperse hollow microspheres is always promising.^{9,22,29–31}

Microfluidics systems are predominantly characterized by laminar flow, resulting in unique fluid morphologies.^{32,33} It enables a continuous operation to produce monodisperse emulsions and is likely to be one of the most promising approaches to produce monodisperse hollow microspheres.^{34,35} Due to the limitations

* Correspondence to: Z Liu, National Engineering Laboratory for Methanol to Olefins, Dalian Institute of Chemical Physics, Chinese Academy of Sciences, Dalian 116023, China. E-mail: liuzm@dicp.ac.cn

a National Engineering Laboratory for Methanol to Olefins, Dalian National Laboratory for Clean Energy, Dalian Institute of Chemical Physics, Chinese Academy of Sciences, Dalian, China

b National Synchrotron Radiation Laboratory, University of Science & Technology of China, Hefei, China

c China University of Chinese Academy of Sciences, Beijing, P. R. China

of raw material for the polymerization or hydrolysis routes so far the applicable hollow materials prepared in microfluidics chip were limited to some specific substances. For example, Steinbacher *et al.* prepared the organosilicon microcapsules with spiny exteriors through the hydrolysis of dichlorodiphenylsilane in a T-junction microfluidic device.³⁶ Eun *et al.* reported the fabrication of hollow TiO₂ microsphere through the controlled hydrolysis of chemical modification metal alkoxides in a co-flow device constructed of two coaxial micro-capillaries.³⁷ Pan *et al.* presented the preparation of monodisperse poly(furfuryl alcohol) hollow microspheres through polymerization in a T-junction device.³⁸ Overall, these were seldom reports of photocatalyst. Therefore, a novel reaction route with efficient, low-cost and facile self-assemble microfluidic synthesis scheme suitable for a broader range of materials, especially for photocatalysis, was very attractive. Herein, we presented a microfluidic-based preparation of uncommon hollow inorganic microsphere from cheap industrial raw materials. These transition metals-based hollow microspheres with a self-assemble Janus shell showed good performance for photocatalysis.

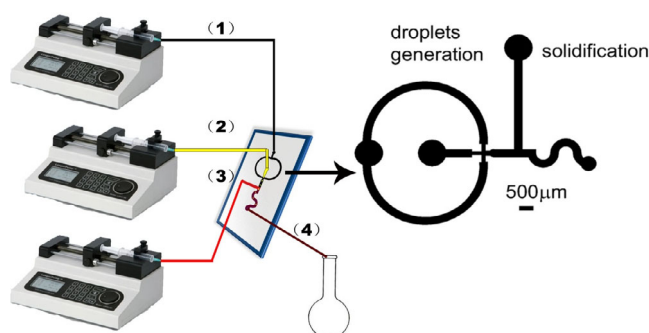


Figure 1. Schematics diagram of microfluidic device. (1) continuous phase; (2) disperse phases; (3) precipitation phase; (4) receiving pipe.

MATERIAL AND METHODS

Chemicals

Cobalt nitrate (Co(NO₃)₂·6H₂O, Tianjin Damao Chemical Reagent Factory, AR); Zinc nitrate (Zn(NO₃)₂·6H₂O, Tianjin Damao Chemical Reagent Factory, AR); Cupric nitrate (Cu(NO₃)₂·3H₂O, Tianjin Damao Chemical Reagent Factory, AR); Polyglycerol polyricinoleate (PGPR, Tianjin Yuchang technology development Co.); Ferrous sulfate (FeSO₄·7H₂O, Tianjin GuangFu Technology development Co., AR); Potassium hydroxide (KOH, Tianjin Damao Chemical Reagent Factory, AR); Triethylamine (TEA, Tianjin Damao Chemical Reagent Factory, AR); Absolute alcohol (Ethanol, Tianjin Fuyu Fine Chemical Co.); Soya-bean oil (Yihai Kerry Limited).

The structure and fabrication of microfluidic chip

Schematics diagram of the microfluidic device used to prepare hollow microsphere was shown in Fig. 1. The microfluidic chip consisted of two units: a flow-focusing region for droplets generation, and a solidification unit for solidifying the droplets. The typical microchannel height of the chip was 150 μm. There were an orifice of 150 μm × 200 μm in size and two nozzles of 150 μm × 150 μm in the flow focusing region, which facilitated the generation of monodisperse droplets. The solidification unit had a nozzle of 150 μm × 300 μm for introducing precipitation phase and a circular arc microchannel of 300 μm × 3 mm for performing precipitation reaction. The chip outlet was connected to a receiving flask with a 20 cm polytene pipe (inner diameter = 0.5 mm).

The polymethylmethacrylate (PMMA) microfluidic device was fabricated by soft lithography combined with microcasting technology. The preparation process was briefly described in three steps. A metal nickel template mold with patterned features was manufactured by microcasting on a nickel substrate with patterned SU-8 photoresist mold fabricated by soft lithography and removing the photoresist. PMMA piece was hot extruded against the mold to copy the microstructure and peeled off from the mold. After drilling connection holes, the patterned PMMA piece was bonded with another PMMA piece with PMMA binder to construct the microfluidic chip.

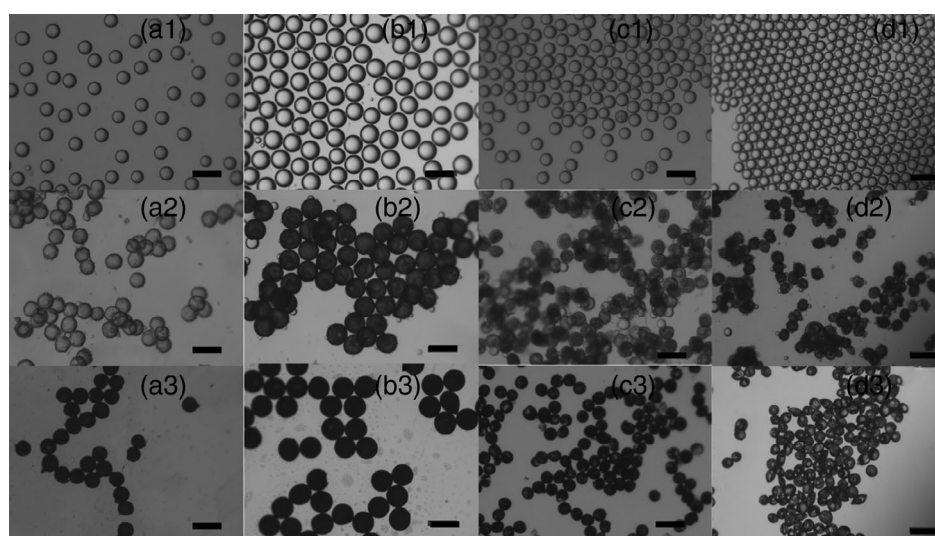


Figure 2. Light microscope images of (1) droplets, (2) solidified droplets, and (3) as-synthesis microsphere prepared with microfluidics chip from precursor solutions containing (a) zinc nitrate, (b) copper nitrate, (c) cobalt nitrate, and (d) ferrous sulfate. The scale bar is 200 μm.

Fluids preparation

The continuous phase (O) was soya-bean oil with 2 wt% PGPR as a surfactant. It was prepared by adding 4.0 g PGPR into 196.0 g commercial soya-bean oil and then stirred for 4 h. The

obtained liquid was filtrated with a 10 μm filter before being used.

The disperse phases (W) were aqueous solutions of certain concentrations of metal salts, such as zinc nitrate, cupric nitrate,

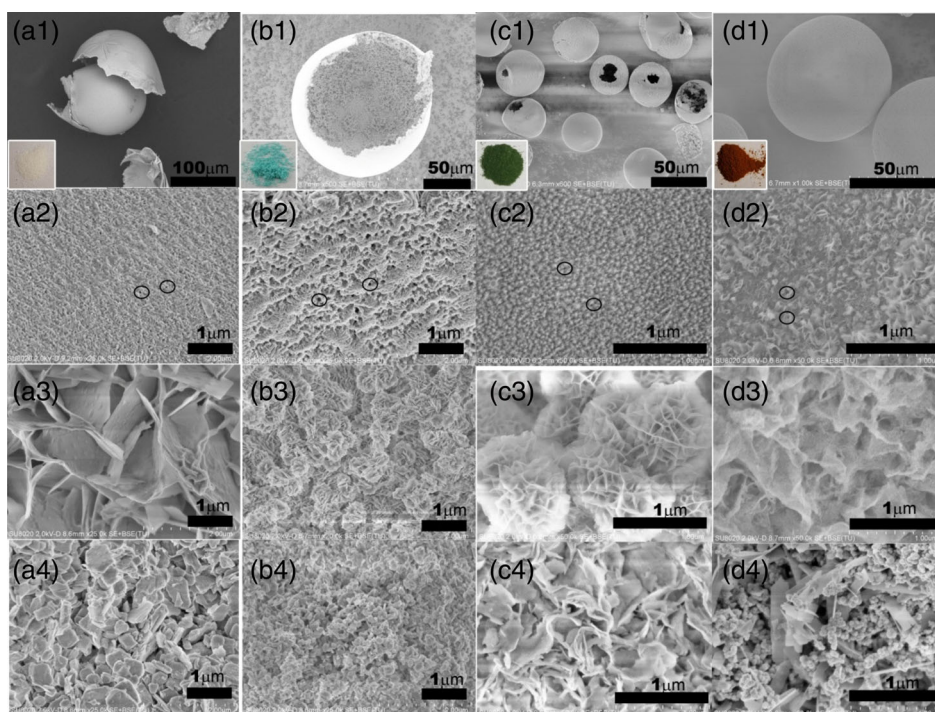


Figure 3. SEM images of (1) overall morphology, (2) outer and (3) inner surface of dried hollow microsphere prepared with microfluidic chip, and (4) the samples prepared in a batch reactor from precursor solutions containing of (a) zinc nitrate, (b) copper nitrate, (c) cobalt nitrate, and (d) ferrous sulfate. The insets in a1, b1, c1 and d1 showed the colors of the microspheres samples.

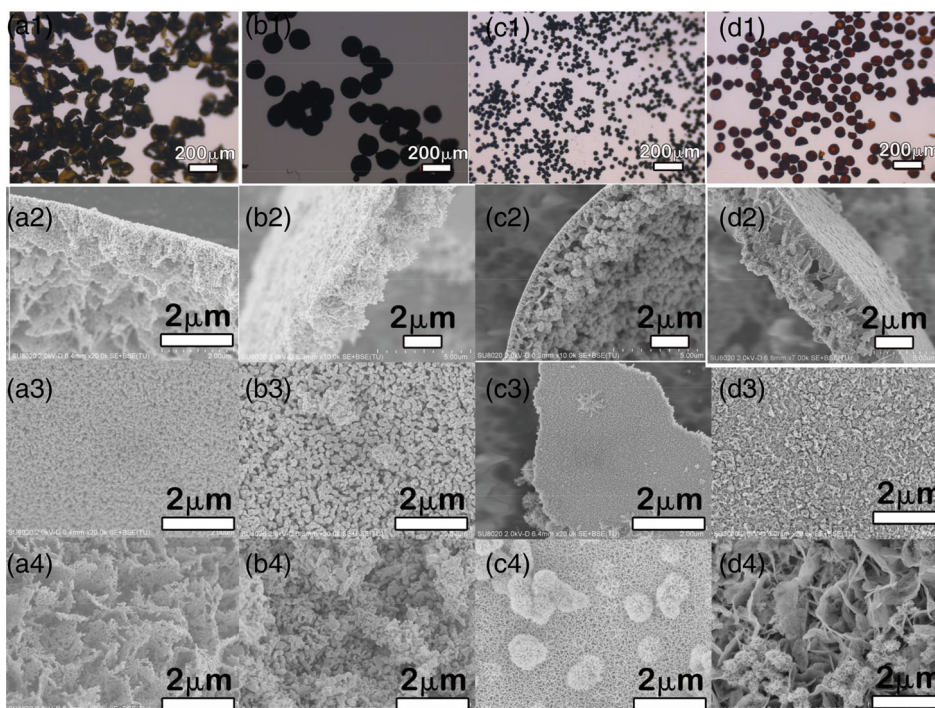


Figure 4. (1) The light microscope of overall morphology and the SEM images of (2) the shell cross-section, (3) outer and (4) inner surface of the calcined hollow samples prepared with microfluidics chip from precursor solutions containing of (a) zinc nitrate, (b) copper nitrate, (c) cobalt nitrate, and (d) ferrous sulfate.

cobalt nitrate, or ferrous sulfate. Quantities of 2.97 g zinc nitrate, 4.83 g cupric nitrate, 5.82 g cobalt nitrate, or 2.78 g ferrous sulfate dissolved into 4.19 g, 7.40 g, 6.44 g or 7.80 g deionized water to obtain aqueous solutions of 2, 2, 2 and 1 mol L⁻¹, respectively. The obtained solutions were filtrated with a 10 μm filter before being used.

The precipitation phase (P) was soya-bean oil containing KOH as a precipitant reagent. For dissolving the inorganic alkali into the oil, a 1 mol L⁻¹ KOH/ethanol solution was used, and simultaneously triethylamine was also added as a solubilizer and secondary precipitant. The typical preparation procedure was described below. A measurement of 2.8 g KOH was dissolved into 35.1 g absolute ethyl alcohol to obtain a 1 mol L⁻¹ KOH/ethanol solution. A quantity of 4.0 g of the above KOH/ethanol solution was mixed with 4.0 g TEA. And then the mixed solution was added into 32.0 g the continuous phase under stirring to obtain a transparent solution with a weight ratio of an ethanol solution of KOH: TEA: soya-bean oil = 1:1:8. The weight percentage of KOH and TEA in the precipitation phase was 0.74 wt% and 10.0 wt%, respectively.

Microfluidics synthesis of hollow microspheres

The microfluidic device was used to prepare the hollow microsphere. Three syringe pumps with a 50 mL syringe were used independently to introduce the fluids into the chip, respectively. In the droplets generation unit, the dispersed phase was cut into monodisperse droplets by the continuous phase through hydrodynamic flow focusing. The obtained emulsion fluid flowed downstream into the solidification unit, wherein the precipitation phase was introduced. The typical flows of dispersed, continuous and precipitation phases were 2, 20, and 40 μL min⁻¹, respectively. The maximum Reynolds number (Re) used in the chip was less than 2. Within seconds of the precipitating event, uniform microcapsules with core-shell morphology were self-assembled based on the monodisperse droplets in the chip device. After aging at room temperature (RT) for 24 h, the precipitate was filtered washed with n-hexane, acetone, alcohol, water, as well as alcohol successively. The washed products were dried at 80 °C under vacuum conditions for 24 h. Their calcined samples were obtained by calcination in a furnace at 450 °C for 4 h, with a ramp rate of 2 °C min⁻¹.

Bulky samples were fabricated in a conventional precipitation method by a batch reactor. The aqueous solutions of raw material were the dispersion phases used in the microfluidic method. The precipitation solutions were the above precipitation phase without soya-bean oil and PGPR surfactant. With two syringe pumps the aqueous solutions and precipitation solutions were separately added drop by drop into the reactor to carry out the precipitation reaction while stirring vigorously. And then the sediments were centrifugally separated, washed with water, and dried at 80 °C under vacuum for 24 h.

Performance evaluation of the photocatalytic activity

The photocatalytic activities of the fresh hollow samples for the degradation of RhB were evaluated through the absorbance of the irradiated solution. In the tests, 5 mg photocatalyst and 5 mL RhB solution with the initial concentration of 10 μmol⁻¹ were dispersed into 95 mL high purity water (18.25 mol L⁻¹ Ω cm in resistivity) in a quartz reactor equipped with an external cooling system. The suspension was magnetically stirred for 20 min to reach the equilibrium of absorption/desorption in the dark, followed by adding 0.255 mL of hydrogen peroxide solution (H₂O₂, 30 wt%). A 300 W xenon lamp (CEL-HXF300E, CEAULIGHT Co.,

Ltd.) equipped with a cut-off filter (420 > nm) was used as a visible-light illumination source. The light intensity in the center position of the reactor was about 100 mW·cm⁻², determined by a Newport optical power/energy meter (842-PE). The degradation reaction was performed under stirring at RT. During the reaction, about 5 mL suspension solution was sampled at 20 min intervals, followed by centrifugation to remove the photocatalyst. The dye concentration of the filtrate was analyzed by the RhB absorption intensity at a UV-vis spectrophotometer (Shimadzu, UV-2600).

Characterization

Scanning electron microscopy images (SEM) were analyzed on a scanning electron microscope (FEI, Quanta 200FEG, accelerating voltage of 20 kV).

X-ray diffraction (XRD) patterns were recorded over a 2θ range of 5° – 80° on an X-ray Diffractometer (PANalytical, X'Pert PRO) by employing Cu Kα radiation (λ = 0.154 nm). The samples were placed onto a glass holder for the experiment.

Thermogravimetric analysis (TGA) was carried on a thermal analyzer (TA, Q600 SDT) under an air atmosphere with a temperature ramp of 20 °C min⁻¹ from 40 to 600 °C.

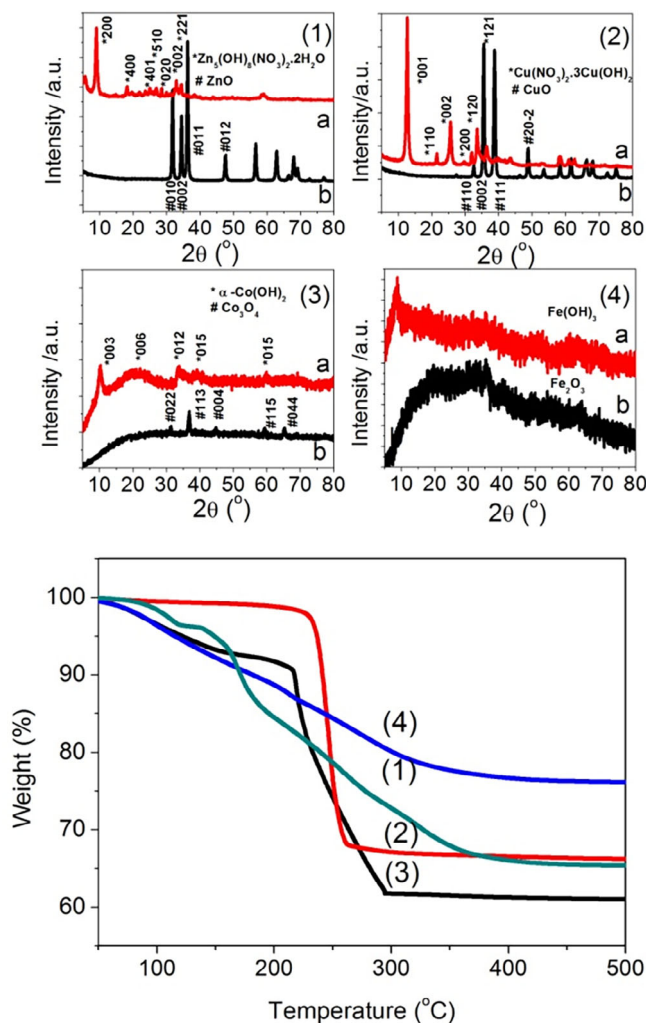


Figure 5. XRD (up) and TGA (down) profiles of (a) fresh and (b) calcined hollow samples prepared from the precursor solutions containing of (1) zinc nitrate, (2) copper nitrate, (3) cobalt nitrate, and (4) ferrous sulfate with microfluidics chip.

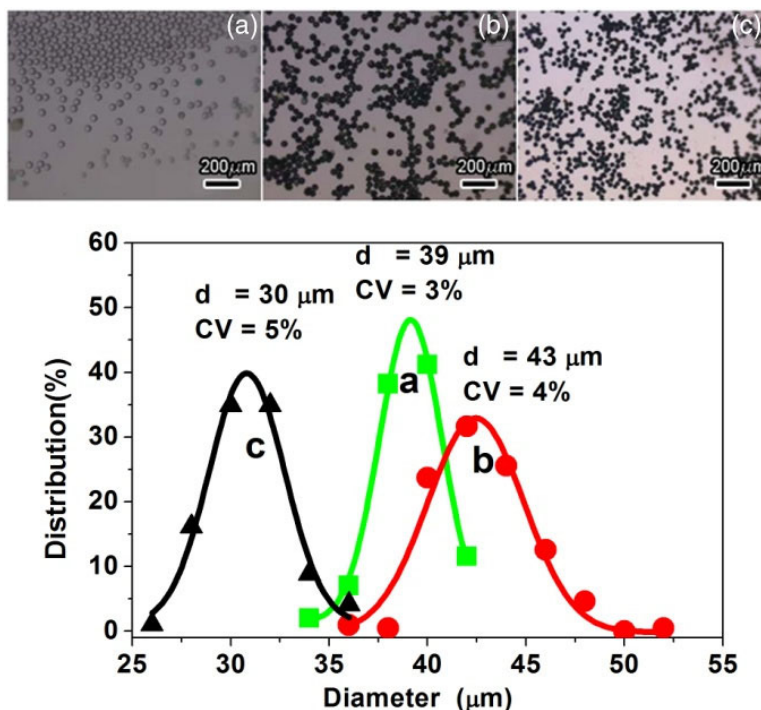


Figure 6. Diameter distributions of (a) droplet, (b) as-synthesis, and (c) calcined microspheres prepared from a precursor solution containing cobalt nitrate.

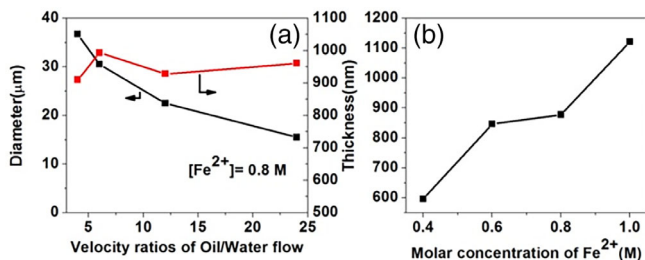


Figure 7. (a) Diameters and shell thickness of hollow microspheres versus velocity ratios of Oil/Water flow; (b) Shell thickness versus molar concentration of metal ions. The start material is a solution of ferrous sulfate.

The mole yield of the metal component was calculated based on the oxide sample calcined at 450 °C with the following expression:

Yield (metallic ion) = (the mole weight of the metal in the calcined oxide) / (the mole weight of the metal in the feed).

Diameters and their distributions of droplet, as-synthesis, and calcined microspheres were obtained from the statistical results over 200 microsphere samples by image measurements.

RESULTS AND DISCUSSION

The microfluidics chip system

The homemade microfluidics chip from PMMA was used due to its good hydrophobicity and resistance for acid, alkaline, and corrosion. It consisted of two functional units: droplet generation and solidification unit. The continuous phase was soya bean oil. The disperse phase was an aqueous solution containing various metal salts, such as zinc nitrate, copper nitrate, cobalt nitrate, or ferrous sulfate. They were obtained by dissolving the raw material into

water, without pH adjustment. The precipitation phase was the soya bean oil containing KOH. For dissolving the inorganic alkali into the oil, the KOH was dissolved in a solution containing ethanol and TEA. The continuous phase and disperse phase were respectively introduced into the chip, and monodisperse aqueous droplets were generated by hydrodynamic flow focusing.³⁹ The emulsion fluid flowed downstream in the microchannel of the chip, wherein the precipitation phase was introduced. A hollow structure of core-shell morphology was self-assembled based on the homogeneous droplets within seconds of the precipitating event in the chip. The PMMA chip itself is hydrophobic and further treatment on its microchannel was not employed. Even with continuous working of about 16 h, the PMMA chip still worked well. All the raw materials used here are commercially available, cheap, and nonreactive in air.

The color changes of droplets

During the solidification reaction, the droplets showed specific color changes according to the precursors. The colorless droplets of zinc nitrate quickly became white particles. And the droplets of copper nitrate were first greener and then formed light blue particles. For the cobalt nitrate, the pink droplet first became deeper and transformed to dark green particles. As for the ferrous sulfate, the pale green droplets quickly changed to white particles of $\text{Fe}(\text{OH})_2$, which further became grey-green. The grey-green particles gradually became brown in air, which was ascribed to the oxidation of Fe^{2+} to Fe^{3+} .

The morphologies of hollow microsphere

The morphologies of droplets, solidified droplets at the chip outlet and as-synthesis particles, produced from various precursor solutions, were characterized by light microscopy (Fig. 2). It revealed all of them were spherical morphology with uniform

diameters of typical dozens of microns. The microsphere samples (named as Zn, Cu, Co, and Fe samples according to the metallic precursors, respectively) were dried under vacuum at 80 °C and their SEM images were shown in Fig. 3. The hollow structure could be observed in broken samples. And the surface morphologies of the external shell were obviously different from that of the inner. The outer showed a smooth surface with massive nanopores, while the inner exhibited a rough morphology with sheet-shaped particles or their constituting flower-like particles rooting vertically from the inside. Due to its thermal instability, structure damage or cracking could be observed after heat drying, especially for the Zn-contained sample. The corresponding control samples were also prepared with a conventional precipitation method in a batch reactor. Their SEM images were also shown in Fig. 3. Compared with the corresponding hollow samples, the accumulation of particles in the bulky samples were more inhomogeneous and disorderly. It was assumed to be related to the droplet-based reactor, wherein the precipitation procedures were essentially identical and controllable in the microfluidics chip. The SEM images of calcined hollow samples were shown in Fig. 4. The inner and outer surfaces retained different morphologies. The smooth outers and the rough inners were inherited from the fresh hollow microspheres. The structural damage caused by calcination could be observed, especially for the ZnO sample, ascribed to violent decomposition.

The XRD and TGA profiles

The XRD and TGA profiles of the hollow samples were shown in Fig. 5. The obtained products were the results of corresponding precipitation reactions. For example, zinc hydroxyl nitrate (JCPDS: 24–1460) and copper hydroxyl nitrate (JCPDS: 15–14) were produced from Zn and Cu nitrate, and α -Co(OH)₂⁴⁰ and amorphous Fe(OH)₃ (oxidized product of Fe(OH)₂) were obtained from cobalt nitrate and ferrous sulfate, respectively. Relevant oxide products could be obtained by the calcination of fresh hollow samples. As shown in TGA profiles, the weight loss after calcination at 500 °C was in the ranges of 24 ~ 39 wt. %.

The diameter distribution

A typical diameter and its distributions of droplets, as-synthesis, as well as calcined microspheres, derived from cobalt nitrate, were shown in Fig. 6. The average diameters were changed from 39 μm of the droplet to 43 μm of as-synthesis sample and 30 μm of calcined one, and the coefficient of variations (CV) of diameter retained about 5%, qualifying as monodisperse. The diameters of as-synthesis samples were larger than that of the droplets, indicating the hydrophilic substance in the precipitation phase, such as ethanol, entered the droplets together with the precipitant.

The diameter and shell thickness regulations

Microsphere size is predominated by the radius of the droplet, which generally depends on several factors, such as interfacial surface tension, coefficient of viscosity, and shear rate.³⁶ Thus microsphere diameter can be facilely adjusted by altering the velocities ratios of continuous and disperse fluid.⁴¹ Fig. 7(a) shows the diameter and total shell thickness of the as-synthesis Fe based hollow microsphere versus the velocities ratios. The diameter decreased with the velocities ratios increment, and the shell thickness did not change much. The effect of the concentration of the metallic ion precursor on the shell thicknesses were shown in Fig. 7(b). The thicknesses increased with concentration raising.

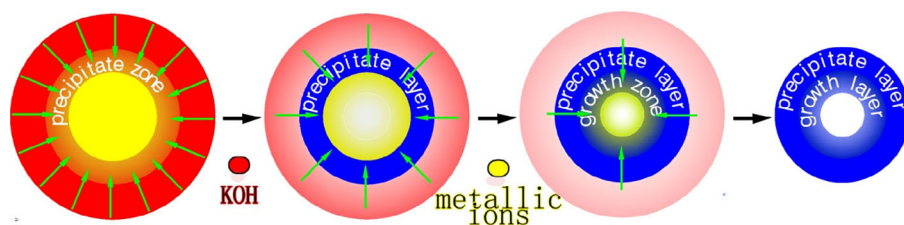
The synthesis mechanism analysis

The droplets were generated and ran downstream the microchannels to the solidification unit in a laminar continuous phase flow with a typical velocity of about 0.8 cm s⁻¹ (Re ≈ 0.15). The solidifying procedure was presumed to undergo two steps: (1) the precipitant first diffused to the water–oil interface of droplets, (2) and then entered the droplets through the interface to react with the reagent in the droplets. The former was considered to be a slowly diffusing step in a laminar fluid of the viscous oil phase, while the latter was much faster in the aqueous microdroplets. Once the precipitant reagent diffused to the interface, therein it could quickly react with the substances in the droplets. Thus, the precipitant reaction preferred to occur at the interface zone of a droplet. At the solidification unit, the precipitant was injected into the microchannel through a micro-nozzle with a higher velocity (1.5 cm s⁻¹) and flow rate (typically twice the emulsion flow). It intensified the precipitant diffusing into the droplet by disturbing the laminar flows, thus an initial shell would be rapidly formed through the precipitation reaction. The effect of gravity sedimentation was neutralized due to the diffusion/convection effect in the microscopic droplets of the microfluidics system. With the accumulation of precipitated colloidal nuclei based on the droplet interface, a spherical shell was constructed

Table 1. The yields of hollow microsphere product

Sample	Yield ^a (%)	Produce ^b (mg h ⁻¹)
Zinc hydroxide nitrate	83	25 ^c
Cupric hydroxide nitrate	71	20 ^c
Cobaltous hydroxide	69	109 ^d
Ferric hydroxide	62	8 ^c

^a Metal mole yields based calcined samples.
^b Dried by vacuum at 80 °C for 24 h.
^c The flux of dispersion phase was 2 μL min⁻¹.
^d the flux of dispersion phase was 10 μL min⁻¹.



Scheme 1. Janus shell formation mechanism of the microcapsules.

within a second nucleation event in the microchannel, forming the smooth outer surface with a large number of piled channels. Afterward, the precipitant reagent still entered into the droplets through the channels. In this stage, the precipitant supply was suppressed due to the impedimental shell. On this condition the reaction was inclined to the nuclei growth rather than nucleation. In general, metallic colloidal particles are positively charged because it could adsorb a metal ion bringing a positive charge. During the solidification procedure, the deepened color of colored droplets also confirmed that the colorful metal ions were absorbed on the initial colloidal shell. The adsorbed metal ions on the inner shell were precipitated preferentially rather than the free ions in the solution. Therefore, sheet-shaped particles or assembling flower-like particles were formed and rooted vertically from the inside shell, constructing the rough inner surface. When performing the precipitation reaction in a batch reactor, the nucleation and the nuclei growth would occur simultaneously in the solution/suspension due to the inhomogeneous reaction condition in a macrosopical environment. Accordingly, heterogeneous and disorderly particles were easily formed. Based on the above analysis, we proposed a two-stage mechanism for the formation of hollow microsphere as showed in **Scheme 1**: First, the colloidal particle derived from the precipitation reaction rapidly constructed the smooth exteriors based on the droplets, and then the colloidal particles directionally grew on the inner shells, resulting in the hollow microspheres with a Janus shell.

The yields of hollow products

The typical yields of various metallic ions were listed in Table 1. The mole yields of metal elements were obtained in the range of 62% to 83% for these hollow samples. With a good yield and an adjustable uniform size, the current method may provide the most promising technique to achieve a goal-directed preparation of a monodisperse hollow microsphere. The preparation of hollow microspheres with the microfluidics technology was operated in a continuous way and a template was not required. Typical productivity with dozens to more than 100 mg per hour by one channel was obtained, depending on the applied conditions. It was competitive with the conventional batch synthesis route, whose typical productivity scale reported was 100 mg per synthesis procedure.⁶ Considering this microfluidics apparatus can be facile to scale-up via simple digital parallelization,^{42,43} it is promising to provide a scalable procedure with such a microfluidic system.

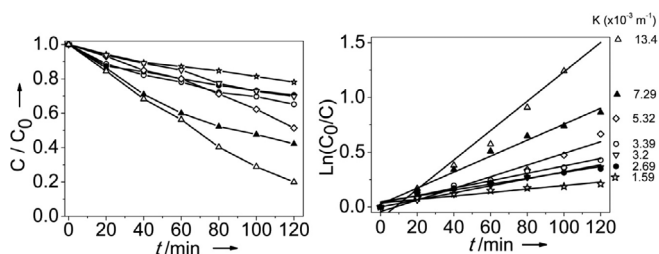


Figure 8. (a) Photodegradation of RhB and (b) the apparent reaction rate constant (k) on Δ Co, \diamond Zn, \circ Fe, and ∇ Cu based fresh hollow microspheres prepared with a microfluidics chip, and on \blacktriangle Co and \bullet Fe based samples prepared by conventional precipitation reaction. (\star : photolysis without a catalyst; Self-photodegradation) Reaction conditions: RhB concentration $0.5 \times 10^{-6} \text{ mol L}^{-1}$, catalyst concentration 0.05 g L^{-1} , H_2O_2 concentration is $2.2 \times 10^{-4} \text{ mol L}^{-1}$, initial pH = 7, 300 W Xe-lamp ($\lambda = 420 \text{ nm}$) with an average light intensity of 100 mW cm^{-2} .

The photocatalytic activities evaluation

The photocatalytic activities of the fresh hollow samples were evaluated for RhB photodegradation under visible-light illumination. The change of RhB relative concentrations as a function of irradiation time were revealed in Fig. 8(a). The apparent reaction rate constants (k) of RhB photodegradation were calculated based on a pseudo-first-order kinetic model and were shown in Fig. 8 (b).^{44,45} For the blank experiment without catalysts, RhB self-degradation was relatively slow. Its k was $1.59 \times 10^{-3} \text{ min}^{-1}$, essential consistency with that ($1.65 \times 10^{-3} \text{ min}^{-1}$) reported by Zhou *et al.*⁴⁴ The degradation rates were promoted with all the catalysts. And the Co hollow catalyst showed the highest degradation activity. The activities were in the sequence of $\text{Co} > \text{Zn} > \text{Fe} > \text{Cu}$ catalyst samples. The photocatalytic activities of two controlled samples, containing Co and Fe respectively, prepared by conventional precipitation method were also tested and shown in Fig. 8. It was noticeable that the Co- and Fe-based hollow samples prepared by microfluidic chip showed better activities (more than 0.84 and 0.26 times respectively) than the corresponding controlled samples. The photocatalytic activities on the oxide samples (namely Co_3O_4 , Fe_2O_3 , and CuO , respectively) derived from the Co-, Fe-, and Cu-based hollow microspheres calcined in air were also evaluated for RhB photodegradation and shown in Fig. 9. They all showed ignorable photocatalytic activities. Significantly, the Co oxide sample showed very low activity although the α - $\text{Co}(\text{OH})_2$ hollow samples had superior activity. The recycling performance of α - $\text{Co}(\text{OH})_2$ hollow catalyst was also tested and shown in Fig. 10. It was revealed that the α - $\text{Co}(\text{OH})_2$ catalyst was recycled. After 5 runs, about 61% catalytic performance was maintained.

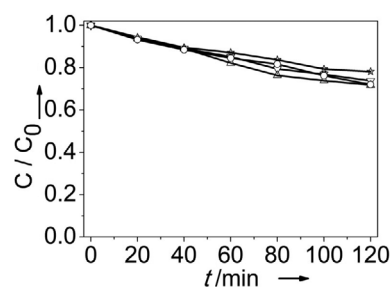


Figure 9. Photodegradation of RhB on the oxides hollow sample of Δ Co, \circ Fe, and ∇ Cu (\star : photolysis without a catalyst; Reaction conditions see Fig. 8).

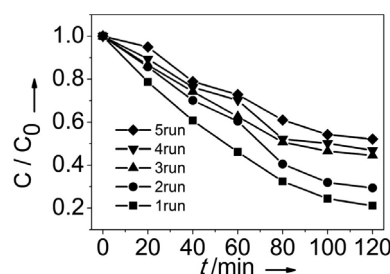


Figure 10. The recycle performance of RhB photodegradation on α - $\text{Co}(\text{OH})_2$ hollow catalyst.

Table 2. The comparison of this work with others

Catalyst	Reaction rate constants k^a ($\times 10^{-3} \text{ min}^{-1}$)	kc^b ($\times 10^{-2} \text{ m}^{-1} \text{ L g}^{-1}$)	Reference
MoS ₂ /MoO ₃ /TiO ₂	108.0	10.8	45
FeOCl	88.2	17.6	48
Nanoplates α -Fe ₂ O ₃	4.4	2.2	44
Nanocubes α -Fe ₂ O ₃	28.2	14.1	44
Nanorods α -Fe ₂ O ₃	73.3	36.6	44
In ₂ S ₃ /KNbO ₃	44.0	7.3	49
Ti/g-C ₃ N ₄	46.1	23.0	50
Cubic ZnTiO ₃	19.0	7.6	51
rGO/ Cubic ZnTiO ₃	65.0	26.0	51
nanorod ZnO	7.7	1.1	52
MXene/nanorod ZnO	24.6	3.6	52
Fe(OH) ₃ hollow sphere	3.4	6.8	This paper
α -Co(OH) ₂ hollow sphere	13.4	26.8	This paper

^a The apparent reaction rate constants (k) of RhB photodegradation were calculated based on a pseudo-first-order kinetic model.
^b kc denotes the rate constant (k) normalized to catalyst concentration, $kc = k$ (catalyst concentration)⁻¹.

In the routes to prepare hollow materials with polymerization, hydrolysis or hydrothermal traditional reaction, due to their harsh reaction conditions, in general oxides products were obtained. Differing from the traditional routes, in the current route the hollow materials were synthesized through the directing precipitation reaction in microcosmic droplets, wherein a controllable reaction condition was readily achieved. Thereby, some hard-to-prepared microspheres, such as hydroxide hollow materials could be synthesized. The photocatalytic activities on the α -Co(OH)₂ hollow catalyst were much better than its oxide sample (namely Co₃O₄ hollow catalyst), suggesting the unique advantage of the current route in the preparation of some uncommon inorganic hollow microspheres.

The shell porosity of the hollow microsphere was intrinsic in the current precipitation route. It was different from the polymerization or hydrolysis synthesis routes, wherein a compact shell tended to be obtained, and thus the substance exchanges inside and outside of microcapsules were hampered. Hollow structures in general can enhance mass transfer. The porous shell was beneficial to the reaction rates by improving mass transport kinetics.^{46,47} Compared to a solid sample with the same mass catalyst, the thin porous shells usually do not cause a severe transport limitation for reagents and products. Besides, different from the agglomerate structures that only small partial incident light is absorbed, the voluminous void space in hollow structures are assumed to improve the overall absorption efficiency through 'light trapping' effects,²⁰ thus the photocatalytic activities of the hollow catalysts can be improved.

The comparisons of this work with others were listed in Table 2. Notable that the normalized rate constant to catalyst concentration ($kc = k$ (catalyst concentration)⁻¹, $6.8 \times 10^{-2} \text{ m}^{-1} \text{ L g}^{-1}$) of the Fe(OH)₃ hollow catalyst herein is thrice that ($2.2 \times 10^{-2} \text{ m}^{-1} \text{ L g}^{-1}$) of Fe based nanoplate catalyst reported by Zhou et al.,⁴⁴ indicating a better photocatalytic activity. Besides, the kc ($26.8 \times 10^{-2} \text{ m}^{-1} \text{ L g}^{-1}$) of the α -Co(OH)₂ hollow catalyst was higher than that of most other catalysts, or was about the same level as that of shape-tuned nanorod Fe based catalyst ($36.6 \times 10^{-2} \text{ m}^{-1} \text{ L g}^{-1}$). It suggested that the α -Co(OH)₂ hollow catalyst was a promising photocatalyst for heterogeneous photo-Fenton oxidation.

CONCLUSIONS

This study presented a novel pathway for the preparation of various transition metal-based hollow microspheres with the different morphology of the inner and outer surface. With microfluidic technology, the inorganic hollow microspheres can be rapid, low-costly, and continuously manufactured through direct precipitation reaction in droplets. The prepared α -Co(OH)₂ hollow microspheres showed promising photocatalytic activity for wastewater treatment based on heterogeneous photo-Fenton oxidation. Furthermore, the current synthesis strategy is universal for the preparation of a variety of metallic-based inorganic hollow microspheres, and is promoting to achieve the goal-directed preparation of a hollow photocatalyst.

ACKNOWLEDGEMENTS

The authors gratefully acknowledge the supports of Natural Science Foundation of China (No. 21376233).

REFERENCES

- Lou XW, Archer LA and Yang ZC, Hollow micro-/nanostructures: synthesis and applications. *Adv Mater* **20**:3987–4019 (2008).
- Hu J, Chen M, Fang XS and Wu LW, Fabrication and application of inorganic hollow spheres. *Chem Soc Rev* **40**:5472–5491 (2011).
- He JH, Chen HM and Zhang L, Inorganic hollow micro/nanospheres. *Prog Chem* **19**:1488–1494 (2007).
- Zhang J, Cao YD, Wang CA and Ran R, Design and preparation of MnO₂/CeO₂-MnO₂ double-shelled binary oxide hollow spheres and their application in CO oxidation. *ACS Appl Mater Inter* **8**:8670–8677 (2016).
- Qi XH, Li XC, He GH, Zhu YZ, Diao YR and Lu HL, Preparation of hollow submicrospheres with ordered porous SiO₂ shell and multiple AuPt nanoalloy cores and their high catalytic activity. *Chem Eng J* **284**: 351–356 (2016).
- Prieto G, Tuysuz H, Duyckaerts N, Knossalla J, Wang GH and Schuth F, Hollow Nano- and Microstructures as catalysts. *Chem Rev* **116**: 14056–14119 (2016).
- Shao PH, Tian JY, Shi WX, Yang Y, Yang X, Gao S et al., Programmable synthesis of metal hydroxide/oxide hollow architectures: towards an efficient and robust photocatalyst for water remediation. *J Mater Chem A* **5**:124–132 (2017).
- Jiang JW, Lim YS, Park S, Kim SH, Yoon S and Piao L, Hollow porous Cu particles from silica-encapsulated Cu₂O nanoparticle aggregates

- effectively catalyze 4-nitrophenol reduction. *Nanoscale* **9**:3873–3880 (2017).
- 9 Yao TJ, Zuo Q, Wang H, Wu J, Xin B, Cui F *et al.*, A simple way to prepare Pd/Fe₃O₄/polypyrrole hollow capsules and their applications in catalysis. *J Colloid Interf Sci* **450**:366–373 (2015).
 - 10 Martinez CJ, Hockey B, Montgomery CB and Semancik S, Porous tin oxide nanostructured microspheres for sensor applications. *Langmuir* **21**:7937–7944 (2005).
 - 11 Yin XM, Li CC, Zhang M, Hao QY, Liu S, Li QH *et al.*, SnO₂ monolayer porous hollow spheres as a gas sensor. *Nanotechnology* **20**:455503 (2009).
 - 12 Bae E, Chah S and Yi JH, Preparation and characterization of ceramic hollow microspheres for heavy metal ion removal in wastewater. *J Colloid Interf Sci* **230**:367–376 (2000).
 - 13 Tian JY, Tian P, Pang HC, Ning G, Bogale RF, Cheng H *et al.*, Fabrication synthesis of porous Al₂O₃ hollow microspheres and its superior adsorption performance for organic dye. *Micropor Mesopor Mat* **223**:27–34 (2016).
 - 14 Zhou L, Zhuang ZC, Zhao HH, Lin MT, Zhao DY and Mai LQ, Intricate hollow structures: controlled synthesis and applications in energy storage and conversion. *Adv Mater* **29**:1602914 (2017).
 - 15 Jiang Z, Huang KH, Yang D, Wang S, Zhong H and Jiang CW, Facile preparation of Mn₃O₄ hollow microspheres via reduction of pentachloropyridine and their performance in lithium-ion batteries. *RSC Adv* **7**:8264–8271 (2017).
 - 16 Yu L, Hu H, Wu HB and Lou XW, Complex hollow nanostructures: synthesis and energy-related applications. *Adv Mater* **29**:1604563 (2017).
 - 17 Li XC, Wang L, Shi JH, Du NX and He GH, Multishelled nickel-cobalt oxide hollow microspheres with optimized compositions and Shell porosity for high-performance Pseudocapacitors. *ACS Appl Mater Inter* **8**:17276–17283 (2016).
 - 18 Longstreet AR and McQuade DT, Organic reaction systems: using microcapsules and microreactors to perform chemical synthesis. *Acc Chem Res* **46**:327–338 (2013).
 - 19 Zhu YF, Shi JL, Li YS, Chen HR, Shen WH and Dong XP, Storage and release of ibuprofen drug molecules in hollow mesoporous silica spheres with modified pore surface. *Micropor Mesopor Mat* **85**:75–81 (2005).
 - 20 Nguyen CC, Vu NN and Do TO, Recent advances in the development of sunlight-driven hollow structure photocatalysts and their applications. *J Mater Chem A* **3**:18345–18359 (2015).
 - 21 Wang XF, Yu R, Wang K, Yang GQ and Yu HG, Facile template-induced synthesis of Ag-modified TiO₂ hollow octahedra with high photocatalytic activity. *Chinese J Catal* **36**:2211–2218 (2015).
 - 22 Du X, He JH and Zhao YQ, Facile preparation of F and N Codoped pinecone-like Titania hollow microparticles with visible light Photocatalytic activity. *J Phys Chem C* **113**:14151–14158 (2009).
 - 23 Li YS and Shi JL, Hollow-structured Mesoporous materials: chemical synthesis, functionalization and applications. *Adv Mater* **26**:3176–3205 (2014).
 - 24 Cai WJ, Wang WQ, Yang YQ, Ren GH and Chen T, Sulfonated polystyrene spheres as template for fabricating hollow compact silver spheres via silver-mirror reaction at low temperature. *RSC Adv* **4**:2295–2299 (2014).
 - 25 Jin Z, Wang F, Wang F, Wang JX, Yu JC and Wang JF, Metal Nanocrystal-embedded hollow Mesoporous TiO₂ and ZrO₂ microspheres prepared with polystyrene Nanospheres as carriers and templates. *Adv Funct Mater* **23**:2137–2144 (2013).
 - 26 Du KF, Cui XD and Tang B, Template-directed synthesis of hollow silica beads by an interfacial sol-gel route. *Chem Eng Sci* **98**:212–217 (2013).
 - 27 Xie F, Qi MZ, Li WJ, Wang K, Yu ZY and Liu B, Classification, fabrication methods and applications of inorganic hollow spheres. *Prog Chem* **23**:2522–2533 (2011).
 - 28 Zhang TR, Zhang Q, Ge JP, Goebel J, Sun M, Yan Y *et al.*, A self-Templated route to hollow silica microspheres. *J Phys Chem C* **113**:3168–3175 (2009).
 - 29 Li D, Qin Q, Duan XC, Yang JQ, Guo W and Zheng WJ, General one-pot template-free hydrothermal method to metal oxide hollow spheres and their Photocatalytic activities and lithium storage properties. *ACS Appl Mater Inter* **5**:9095–9100 (2013).
 - 30 Chen ZT, Niu DC, Li YS and Shi JL, One-step approach to synthesize hollow mesoporous silica spheres co-templated by an amphiphilic block copolymer and cationic surfactant. *RSC Adv* **3**:6767–6770 (2013).
 - 31 Feng ZG, Li YS, Niu DC, Li L, Zhao W, Chen H *et al.*, A facile route to hollow nanospheres of mesoporous silica with tunable size. *Chem Commun* **23**:2629–2631 (2008).
 - 32 Dreyfus R, Tabeling P and Willaime H, Ordered and disordered patterns in two-phase flows in microchannels. *Phys Rev Lett* **90**:144505 (2003).
 - 33 Thorsen T, Roberts RW, Arnold FH and Quake SR, Dynamic pattern formation in a vesicle-generating microfluidic device. *Phys Rev Lett* **86**:4163–4166 (2001).
 - 34 Wang WT, Chen R, Xu JH, Wang YD and Luo GS, One-step microfluidic approach for controllable production of gas-in-water-in-oil (G/W/O) double emulsions and hollow hydrogel microspheres. *RSC Adv* **4**:16444–16448 (2014).
 - 35 Gokmen MT, De Geest BG, Hennink WE and Du Prez FE, "Giant" hollow multilayer capsules by microfluidic templating. *ACS Appl Mater Inter* **1**:1196–1202 (2009).
 - 36 Steinbacher JL, Moy RWY, Price KE, Cummings MA, Roychowdhury C, Buffy JJ *et al.*, Rapid self-assembly of core-shell organosilicon microcapsules within a microfluidic device. *J Am Chem Soc* **128**:9442–9447 (2006).
 - 37 Eun TH, Kim SH, Jeong WJ, Jeon SJ, Kim SH and Yang SM, Single-step fabrication of Monodisperse TiO₂ hollow spheres with embedded nanoparticles in microfluidic devices. *Chem Mater* **21**:201–203 (2009).
 - 38 Pan YC, Ju MH, Wang C, Zhang LX and Xu NP, Versatile preparation of monodisperse poly(furfuryl alcohol) and carbon hollow spheres in a simple microfluidic device. *Chem Commun (Camb)* **46**:3732–3734 (2010).
 - 39 Anna SL, Bontoux N and Stone HA, Formation of dispersions using "flow focusing" in microchannels. *Appl Phys Lett* **82**:364–366 (2003).
 - 40 Liu ZP, Ma RZ, Osada M, Takada K and Sasaki T, Selective and controlled synthesis of alpha- and beta-cobalt hydroxides in highly developed hexagonal platelets. *J Am Chem Soc* **127**:13869–13874 (2005).
 - 41 Umbanhowar PB, Prasad V and Weitz DA, Monodisperse emulsion generation via drop break off in a coflowing stream. *Langmuir* **16**:347–351 (2000).
 - 42 Kim JH, Choi WC, Kim HY, Kang Y and Park YK, Preparation of monodispersed mixed metal oxide micro hollow spheres by homogeneous precipitation in a micro precipitator. *Powder Technol* **153**:166–175 (2005).
 - 43 Vladisavljevic GT, Khalid N, Neves MA *et al.*, Industrial lab-on-a-chip: design, applications and scale-up for drug discovery and delivery. *Adv Drug Deliver Rev* **65**:1626–1663 (2013).
 - 44 Zhou X, Lan J, Liu G, Deng K, Yang Y, Nie G *et al.*, Facet-mediated photodegradation of organic dye over hematite architectures by visible light. *Angew Chem Int Ed Engl* **51**:178–182 (2012).
 - 45 Li ZY, Cao F, Wang L, Chen ZW and Ji XH, A novel ternary MoS₂/MoO₃-TiO₂ composite for fast photocatalytic degradation of rhodamine B under visible-light irradiation. *New J Chem* **44**:537–542 (2020).
 - 46 De Rogatis L, Cargnello M, Gombac V, Lorenzuti B, Montini T and Fornasiero P, Embedded phases: a way to active and stable catalysts. *ChemSusChem* **3**:24–42 (2010).
 - 47 Fang YJ, Wang YW, Gu L, Lu R and Sha J, Effect of the defect on photoluminescence property of Al-coated ZnO nanostructures. *Opt Express* **21**:3492–3500 (2013).
 - 48 Zhang BY, Chen MD, Li DY, Xu HM and Xia DS, Quantitative investigation into the enhancing utilization efficiency of H₂O₂ catalyzed by FeOCl under visible light. *J Photoch Photobio A* **386**:112072 (2020).
 - 49 Xu JJ, Liu C, Niu JF and Chen MD, Preparation of In₂S₃ nanosheets decorated KNbO₃ nanocubes composite photocatalysts with significantly enhanced activity under visible light irradiation. *Sep Purif Technol* **230**:115861 (2020).
 - 50 Zhang RY, Niu SY, Zhang XC, Jiang ZY, Zheng JM and Guo CF, Combination of experimental and theoretical investigation on Ti-doped g-C₃N₄ with improved photo-catalytic activity. *Appl Surf Sci* **489**:427–434 (2019).
 - 51 Li JS, Cui HT, Mu DY *et al.*, Synthesis and characterization of rGO decorated cubic ZnTiO₃ rods for solar light-induced photodegradation of rhodamine B. *New J Chem* **43**:3374–3382 (2019).
 - 52 Liu XY and Chen CS, Mxene enhanced the photocatalytic activity of ZnO nanorods under visible light. *Mater Lett* **261**:127–127 (2020).